

Fish Gelatin-based Films for Gas Sensing

Inês Pimentel Moreira^a, Laura Sato, Cláudia Alves, Susana Palma^b and Ana Cecília Roque^c

UCIBIO, Chemistry Department, School of Science and Technology, NOVA University of Lisbon,
2829-516 Caparica, Portugal

Keywords: Gas-sensing, Electronic Nose, Fish Gelatin, Liquid Crystal, Ionic Liquid, Volatile Organic Compounds.

Abstract: Electronic noses (e-noses) mimic the complex biological olfactory system, usually including an array of gas sensors to act as the olfactory receptors and a trained computer with signal-processing and pattern recognition tools as the brain. In this work, a new stimuli-responsive material is shown, consisting of self-assembled droplets of liquid crystal and ionic liquid stabilised within a fish gelatin matrix. These materials change their opto/electrical properties upon contact with volatile organic compounds (VOCs). By using an in-house developed e-nose, these new gas-sensing films yield characteristic optical signals for VOCs from different chemical classes. A support vector machine classifier was implemented based on 12 features of the signals. The results show that the films are excellent identifying hydrocarbon VOCs (toluene, heptane and hexane) (95% accuracy) but lower performance was found to other VOCs, resulting in an overall 60.4% accuracy. Even though they are not reusable, these sustainable gas-sensing films are stable throughout time and reproducible, opening several opportunities for future optoelectronic devices and artificial olfaction systems.

1 INTRODUCTION

Artificial olfaction mimics the sense of smell in humans, which relies on complex systems that start with a binding event of odours to an array of olfactory receptors and finish with signal processing and pattern recognition by the brain (Gutiérrez & Horrillo, 2014). Electronic noses (e-noses) have arisen as an emerging tool for the detection of odours – sets of volatile organic compounds (VOCs) – in several areas such as medicine, food quality or environment (Barbosa et al., 2018). Since the traditionally used gas sensors in e-noses are metal oxide semiconductors or synthetic conducting polymers and both present several drawbacks (Baldwin et al., 2011), there is a continuous search for alternative gas-sensing materials.

Liquid crystals (LC) are unique responsive materials due to their ability to change molecular order as a response to chemical and physical *stimuli*, with a long history in a variety of technologies. The design of LC materials that respond to targeted biological or chemical species has more recently

arisen for gas sensing technologies (Carlton et al., 2013). This is made possible due to the high sensitivity of the LC ordering to molecular-level events, endowing the amplification of small changes into optical responses (Shibaev et al., 2015).

Ionic liquids (IL) have also been explored as gas sensing materials, due to their negligible vapour pressure and high ionic conductivity (IC) (Rehman & Zeng, 2015). They are known as designer solvents, as the choice of the cation and anion endows some tunability from a large structural and functional diversity (Meng et al., 2012). Different ionic liquids have been combined with gelatin to make ionogels as chemiresistive gas sensors (Carvalho et al., 2014). More recently, a new type of gas sensors composed of self-assembled droplets of LC and IL stabilised within a polymeric matrix has been reported (Hussain et al., 2017). These materials change their opto/electrical properties in the presence of VOCs and can be used as sensing elements in an e-nose. A study on LC/IL droplets embedded in bovine gelatin showed that such materials can accurately classify 11 distinct VOCs (Esteves et al., 2019). Gelatin is achieved from the partial hydrolysis of the fibrous

^a  <https://orcid.org/0000-0002-5502-091X>

^b  <https://orcid.org/0000-0002-1851-8110>

^c  <https://orcid.org/0000-0002-4586-3024>

protein collagen, the principal constituent of animal skin, bone and connective tissue (Karim & Bhat, 2009). Gelatin from marine sources has gained importance as it appeared as an alternative to bovine gelatin, associated with the Bovine Spongiform Encephalopathy crisis. Additionally, the demand for non-bovine and non-porcine gelatin has increased due to religious and social reasons (Sarbon et al., 2013).

This work shows that fish gelatin is a valuable alternative to bovine gelatin for the immobilization of LC/IL droplets, yielding stable gas-sensing materials with VOC-classification ability. Such information will be beneficial for the future assembly of an array of materials for sensing complex mixtures of VOCs.

2 MATERIALS & METHODS

2.1 Materials

Gelatin from cold water fish skin was purchased from Sigma-Aldrich. The ionic liquid 1-Butyl-3-methylimidazolium dicyanamide [BMIM][DCA] (>98%) was purchased from IoLiTec (Germany) and the liquid crystal 4-Cyano-4'-pentylbiphenyl (5CB) (> 98%) from TCI Chemicals (Belgium). The solvents dichloromethane and hexane were purchased from VWR, ethanol (purity $\geq 99.8\%$) was purchased from Sigma-Aldrich. Acetonitrile (purity $\geq 99.9\%$), chloroform, diethyl ether (HPLC grade), ethyl acetate, heptane, methanol (HPLC grade) and toluene were supplied by Fisher Scientific. Acetone (purity $\geq 99.5\%$) was purchased from Honeywell and isopropanol (purity $\geq 99.5\%$) from ROTH. All solvents were used as purchased.

2.2 Film Preparation

[BMIM][DCA], 5CB, fish gelatin and milliQ water were mixed as previously reported (Hussain et al., 2017). Gelatin from bovine skin (gel strength ≈ 225 g; Bloom Type B) normally presents a larger concentration of proline and hydroxyproline when compared to gelatin from cold water fish (Karim & Bhat, 2009), which is key for the stabilisation mechanism (Joly-Duhamel et al., 2002). The amount added of each reagent was adjusted to ensure proper gelification.

The gel was then spreaded into films on top of microscope glass slides with an automatic film applicator (TQC, The Netherlands) and a quadruplex VF2168-043 at a defined $15 \mu\text{m}$ thickness. Three negative control gels (C0, C1 and C2) were prepared by following the same procedure described above, but

without including in the composition the ionic liquid and the liquid crystal (C0), the liquid crystal (C1), or the ionic liquid (C2). In the absence of ionic liquid, its volume was replaced by milliQ water. All films were left to stand at room temperature for at least 24 hours before used.

2.3 Film Characterisation

The films were observed using an optical microscope (Axio Observer.Z1/7) (Zeiss, Germany) coupled with an AxioCam 503 color camera. For the morphological characterisation of LC droplets, images were taken under crossed (90°) polarizers, giving polarised optical microscopy (POM) images. ZEN 2.3 software (ZEN Pro) was used for microscope control, image acquisition and processing. The magnification used was 100x.

A black mask with a 5 mm circular hole was applied on the bottom of each glass slide where the film was spreaded, in order to delimit the analysis area to VOC exposure. The panoramic polarised optical microscopy (POM) image of this circular area was taken using the *Tiles* module within ZEN software and a 100x magnification. The mean grey value of the circular area was then measured using the tools of FIJI distribution (Schindelin et al., 2012) of ImageJ open software (Rueden et al., 2017) by calculating the grey pixels over the total pixels in the grey-scale image.

2.4 Acquisition of Optical Signals upon Exposure to VOCs

3 selected films were placed in an in-house built e-nose, to study their optical responses to VOC exposure. The 3 different controls were also added, filling the 6-sensor slot chamber. Within these films, the LC molecular rearrangement upon exposure of sensing films to VOCs is what gives an optical signal (Figure 1a), which can thus be analysed. As previously described in (Hussain et al., 2017; Santos et al., 2019), each slot in the detection system is composed of a light emitting diode (LED), a sensing film sandwiched between two crossed polarizers (90°) and a light dependent resistor (LDR) (which is represented in Figure 1b). The LC is arranged in radial configuration when the films are exposed to air (Figure 1c), being able to rotate the plane of the incident polarized light, which allows it to cross the second polarizer and reach the LDR (Figure 1b). However, the presence of a VOC analyte triggers the LC configuration to switch from radial to isotropic

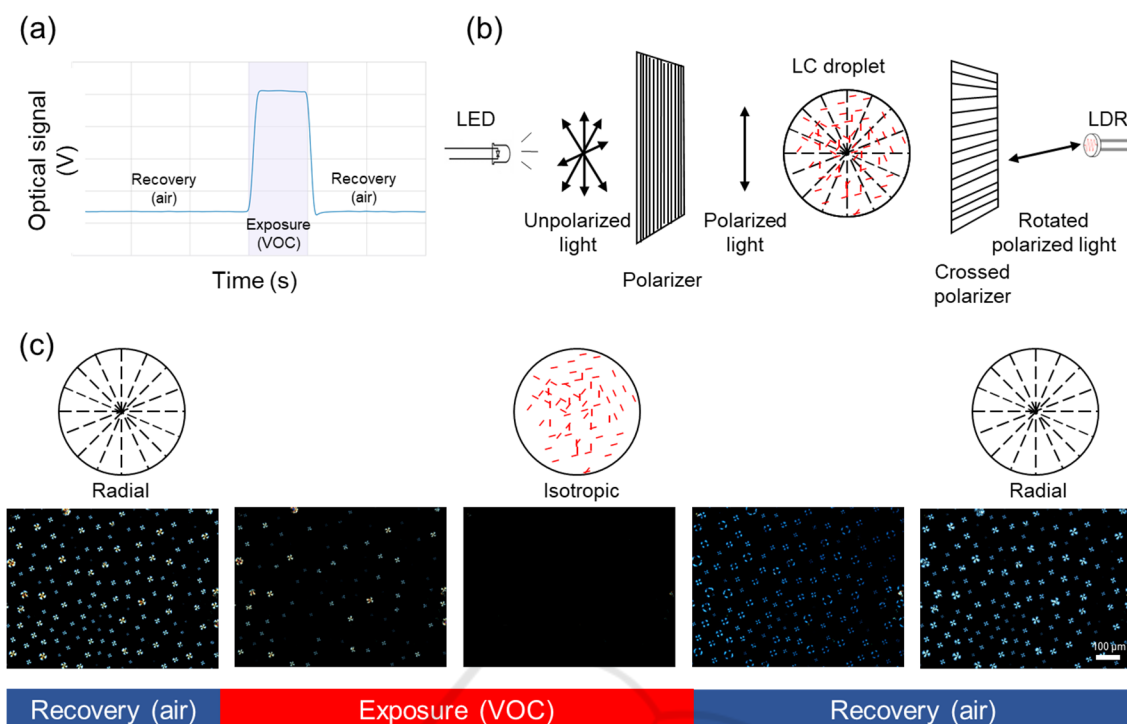


Figure 1: (a) Characteristic optical signal given by the e-nose (upon exposure to hexane, in the example); (b) Schematic representation of the e-nose working mode, with the film sandwiched between two crossed polarizers: the signal is thus given by the inability of light to cross the second crossed polarizer when radial-to-isotropic configuration change happens. (c) Schematic representation of liquid crystal/ionic liquid droplets with LC in radial and isotropic configuration, together with polarised optical microscopy images of the hybrid gels recorded in real time upon exposure to hexane and recovery with air.

(Figure 1c), losing the ability to rotate the plane of polarized light and thus hindering light to pass through the second polarizer (Figure 1b).

The sensing films were exposed to a sequence set of 11 VOCs, with increased polarity (see partition coefficients in Table 1). Before starting any experiment, pure solvents were heated up to 37°C for 15 min in a sample vial to ensure headspace saturation. The resulting gas in the headspace was then pumped through the sensors, using cycles of 5 seconds exposure to VOC and 15 seconds recovery with air, for a total of 15 minutes (45 sequential cycles). Optical signals were acquired at a sampling rate of 90 Hz. Different batches of films were produced so that triplicates were analysed and reproducibility was assured. Each film was characterised before and after the exposure to the set of 11 VOCs.

2.4.1 Signal Processing and Automatic VOC Classification

Twelve features were extracted from each cycle of the optical signals and used as input variables to build an automatic VOC classifier algorithm based on support

Vector Machine (SVM). The chosen features were the ones that gave the best performances, as reported in (Santos et al., 2019). Data from three film batches were used to train, so that the SVM classifier could learn a VOC classification model. Testing was performed using data from a fourth film batch. The normalised classification results were presented in a confusion matrix (in percentage).

Table 1: Set of 11 VOCs, divided by chemical class, chemical structure and partition coefficient ($\log P$) properties.

Chemical class	VOC	Structure	$\log P$
Hydrocarbons	Heptane	<chem>CCCCCCC</chem>	3.42
	Hexane	<chem>CCCCCC</chem>	3
Aromatic hydrocarbons	Toluene	<chem>Cc1ccccc1</chem>	2.52
Chlorinated	Chloroform	<chem>ClC(Cl)Cl</chem>	1.67
	Dichloromethane	<chem>ClC(Cl)C</chem>	1.01

Table 1: Set of 11 VOCs, divided by chemical class, chemical structure and partition coefficient ($\log P$) properties (cont.).

Ethers	Diethyl ether		0.76
Esters	Ethyl acetate		0.29
Ketones	Acetone		0.2
Nitrogenated	Acetonitrile		0.17
Alcohols	Ethanol		0.07
	Methanol		-0.27

3 RESULTS AND DISCUSSION

3.1 Characterisation of Gas-sensing Films

Before using the films made of 5CB/[BMIM][DCA] droplets immobilised in a fish gelatin matrix as sensors for pure VOCs, they were characterised and studied.

3.1.1 Stability over Time

Polarised optical microscopy (POM) was used to characterise the morphology of the sensing films. The images show that it was possible to produce

homogeneous films filled with LC/IL droplets stabilised by the fish gelatin matrix (Figure 2a). The film stability over time was studied by following the same region of interest (ROI) throughout 1 month of storage at room temperature and humidity, taking images each 1 week (Figure 2a-e).

The first and last images were aligned with ImageJ, overlapped and then processed by a Python script to compare them (Figure 2f). It was possible to conclude that the films were stable after 1 month of storage, since they remained in the same positions, with just some fluctuations in size due to humidity changes in the laboratory. However, in the following works, the relative humidity must be controlled to ~50% until all film characterisation and smelling experiments are complete.

3.1.2 Optically Active Area and Signal Baseline

The delimited circular area of all the gas-sensing films was analysed in the polarised optical microscope before using them as sensors for the set of 11 VOCs. There can be some variability in the spreading of the gel, producing slightly different films within the same gel batch. The presence of less droplets within the specific 5 mm circular area (as for the film in Figure 3a compared with the one in Figure 3c) lowers the brightness of the film (as calculated via the mean grey value). A lower mean grey value results in higher baselines of the optical signals (Figure 3d), which will consequently affect the signal amplitude.

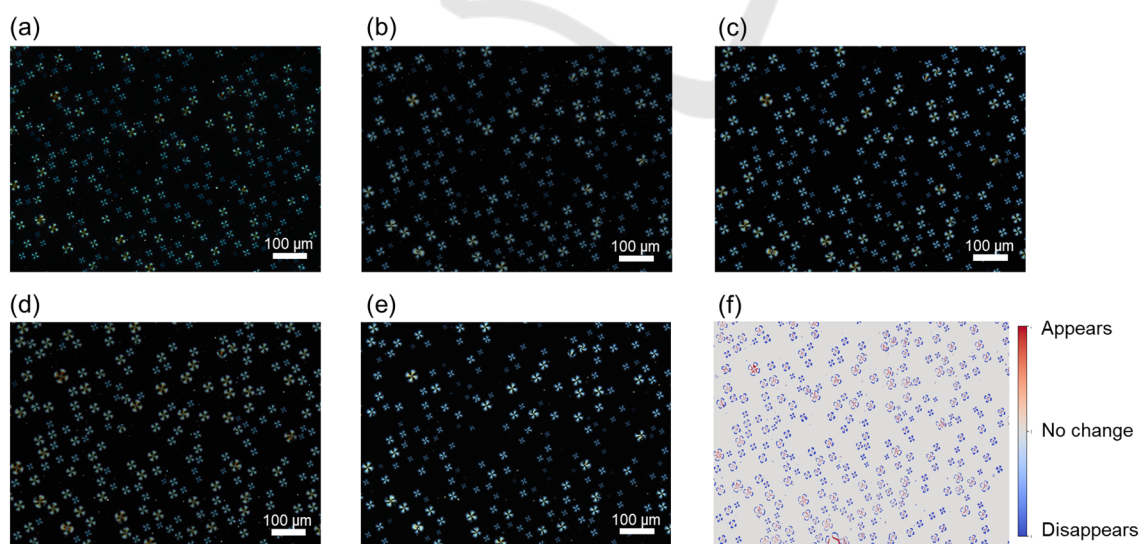


Figure 2: Polarised optical microscopy images of the same area 1 day (a), 1 week (b), 2 weeks (c), 3 weeks (d), 4 weeks (e) after preparation; Changes on the morphology between images a and e, after superimposed and analysed (f).

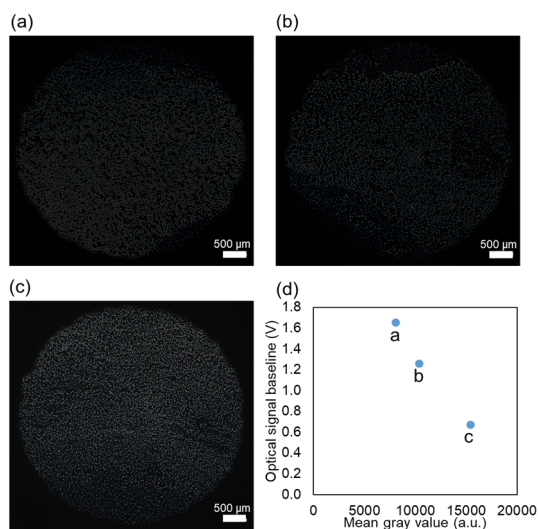


Figure 3: Panoramic polarised optical microscopy image of the whole optically-active area from 3 exposed films of the same batch (a-c); Correlation between the optical signal baseline observed from the e-nose and the mean grey value taken from the tiles above (d).

3.2 Optical Response to VOCs

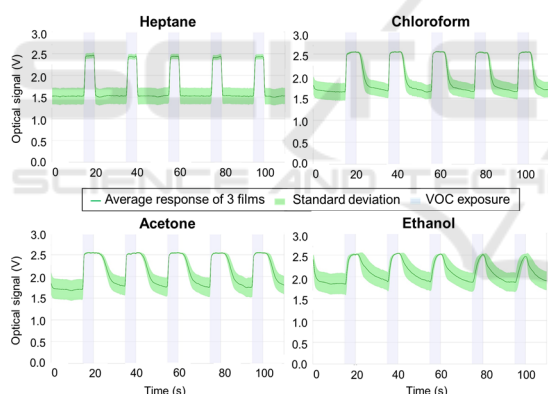


Figure 4: Optical signals (average of 3 films from the same batch of fish-gelatin based gas-sensing films) upon exposure to heptane, chloroform, acetone and ethanol.

The standard deviation of the average optical signal (Figure 4) achieved from the 3 films of the same batch is due to the slight variability in their optically active area, as previously mentioned (Figure 3). The optical signals differ for different VOCs (Figure 4), which is explained by the affinity each of them presents to the liquid crystal, ionic liquid or even biopolymeric matrix that compose the films. When using these fish gelatin-based sensors, the characteristic signal of heptane is rectangular-shaped, which probably occurs due to a quick effect on the LC configuration change

upon exposure and consecutive recovery with air. On the other hand, ethanol follows more of a triangular-type shape, which can be related to the tendency of its hydroxyl group (Table 1) to interact with the fish gelatin by hydrogen bonds. This competitive action of ethanol into droplets or into the biopolymeric matrix can possibly explain the slower radial-to-isotropic and isotropic-to-radial configuration change, or the destabilisation of the droplets within the matrix.

3.2.1 VOC Signature and Discrimination Ability

The characteristic signals yielded by the films allow for a distinction ability between VOC chemical classes. The performance of the classifier (accuracy % of VOC prediction) is presented in a confusion matrix (Figure 5), whereby the blue squares in the diagonal represent the correct VOC prediction accuracies. The best performance is achieved when predicting the most hydrophobic volatiles (hydrocarbons), distinguishing satisfactorily the heptane, hexane and toluene (95% accuracy, in average). In what concerns the alcohols, the accuracy is not as high but it confuses only between ethanol and methanol, which suggests that it is a good prediction tool for VOC chemical classes.

		Predicted										
		Heptane	Hexane	Toluene	Chloroform	Dichloromethane	Diethyl ether	Ethyl acetate	Acetone	Acetonitrile	Ethanol	Methanol
Actual	Heptane	93	7	0	0	0	0	0	0	0	0	0
	Hexane	2	98	0	0	0	0	0	0	0	0	0
	Toluene	0	0	94	0	5	1	0	0	0	0	0
	Chloroform	0	0	0	58	3	0	16	0	23	0	0
	Dichloromethane	0	3	20	0	9	67	1	0	0	0	0
	Diethyl ether	0	31	6	0	3	60	0	0	0	0	0
	Ethyl acetate	0	0	30	3	27	2	33	0	5	0	0
	Acetone	0	0	0	4	0	0	22	8	66	0	0
	Acetonitrile	0	0	0	2	0	0	0	1	96	0	1
	Ethanol	0	0	0	0	0	0	0	0	0	55	45
	Methanol	0	0	0	0	0	0	0	0	1	39	60

Figure 5: Confusion matrix for implemented SVM-based classifier, representing the prediction results for 11 VOCs. The blue squares represent the frequency of correct predictions and grey squares the frequency of failed predictions (in percentage). Overall accuracy represents the average frequency of correct predictions, calculated as the average of the blue squares: 60.36%.

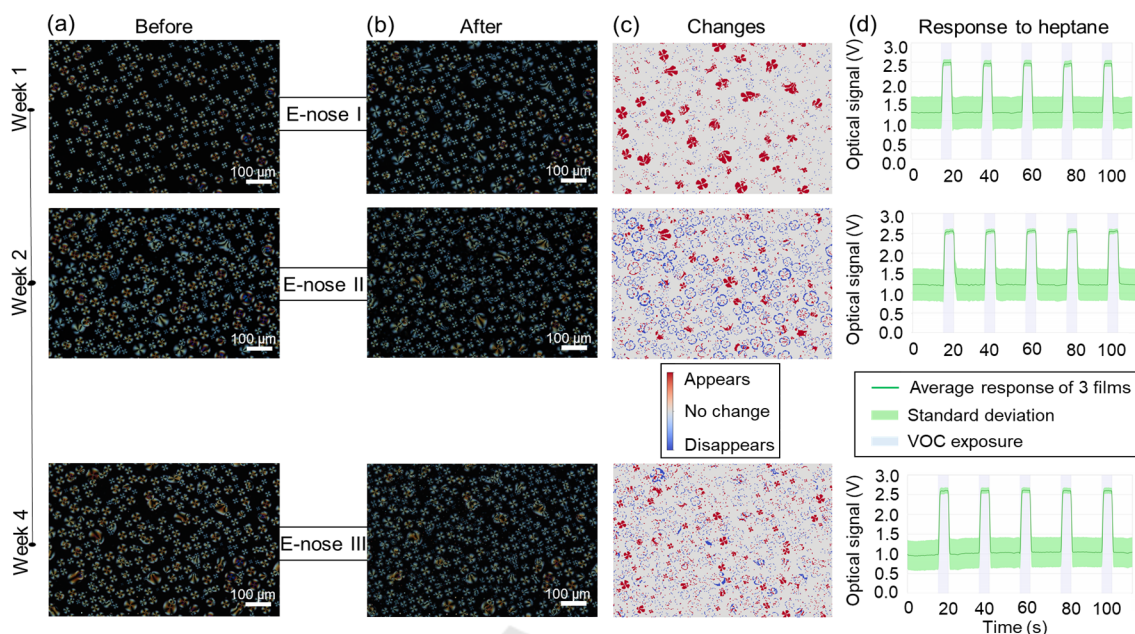


Figure 6: Polarisated optical microscopy images of the same region of interest before (a) and after (b) each e-nose experiment performed with the same gas-sensing films 1 week after preparation, 2 weeks and 4 weeks. (c) Changes on the morphology between images a and b and for each e-nose experiment, after superimposed and analysed. (d) Response to heptane for each of the e-nose experiments.

3.3 Sensor Reusability Capability

The same films were then exposed to the sequence of 11 VOCs a second and a third time, in order to study their reusability capability. The sensing experiments on the same films were performed 1, 2 and 4 weeks after their production (Figure 6). When analysing the morphological images of the same ROI before (Figure 6a) and after (Figure 6b) each e-nose experiment, it is obvious that the largest change happened after the first experiment in the first week (Figure 6c). Even though the response to heptane is quite similar in all the repeated e-nose experiments (Figure 6d), the films change after exposed for the first time and do not show the exact same optical signals. In fact, the overall prediction accuracy decreased from 60.36 to 30.3% on the second exposure, but it increased again to 45.8% on the third exposure. Since the prediction accuracies upon a second and third exposure vary, they cannot be reused, unless the environmental conditions are tightly controlled to avoid droplet swelling and shrinking with relative humidity fluctuations. Even though the sensing films, in general, decreased their ability to discriminate VOCs upon sequential exposures, chloroform, *e.g.*, showed an increasing accuracy prediction (Figure 7). In fact, some VOCs as chloroform or ethanol overtook the 60% accuracy threshold after being exposed more than once.

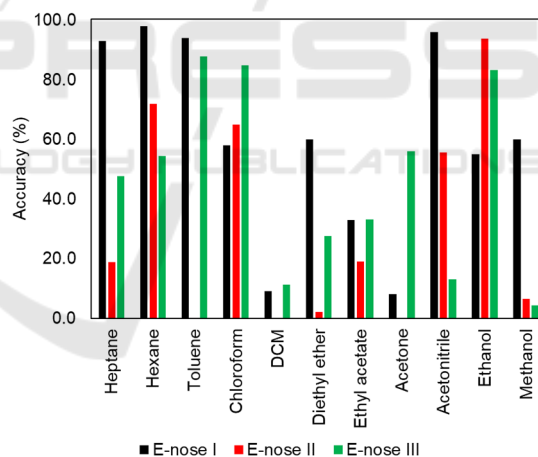


Figure 7: Comparison of prediction accuracies, for each VOC, between the first e-nose experiment (as in the presented confusion matrix) and the 2 next e-nose experiments. Overall accuracies are 60.36, 30.3% and 45.8% for the first, second and third exposures.

3.4 Control Films

The response to VOCs given when using control films as sensors was significantly different from the gas-sensing films shown before (Figure 4). Controls C0 and C1 do not possess liquid crystal in their composition and thus do not respond to any VOCs, presenting a flat line signal (only one example shown

for heptane in Figure 8a). The POM images using crossed polarizers show nothing (Figure 8b-c), exactly due to the absence of birefringence. The control C2, which has liquid crystal but no ionic liquid, is able to detect the presence of VOCs, even though its response is weaker than the ones given from the gas-sensing films (Figure 4). The former presents a lower signal amplitude than the latter, since the C2 is overall darker (Figure 8d) than the sample with ionic liquid (Figure 2a). This lower mean grey value results in a higher baseline, as explored in Figure 3d. The absence of ionic liquid results in droplets that are not based on radial LC configuration, which gives this control some variability and non-consistency. It is possible to conclude from the confusion matrix (not shown) that this control has lower prediction accuracy than the samples with ionic liquid. The importance of the ionic liquid, as well as all the other components in the gas-sensing films, is reiterated for the optical mechanism optimisation of the e-nose.

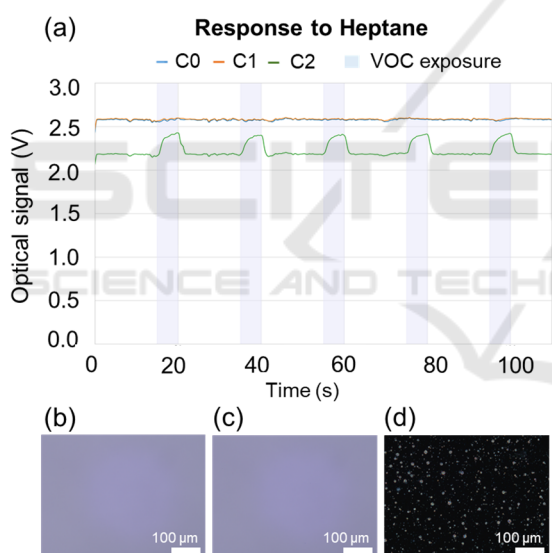


Figure 8: Optical response when using the controls as sensing films (heptane as an example) (a); Representative POM images of the three controls: (b) C0 fish gelatin + water; (c) C1 fish gelatin + IL + water; (d) C2 fish gelatin + LC + water.

3.5 Comparison to Bovine Gelatin-based Sensing Films

Fish gelatin-based sensing films appear as a promising alternative to bovine gelatin-based sensing films as they showed more homogeneous results and lower variability to VOC prediction when comparing different batches. Since independent validation was used in this work, it would not be realistic to compare

the presented confusion matrix (Figure 5) with the previously reported ones for bovine gelatin-based films in (Esteves et al., 2019; Santos et al., 2019), that used 10-fold cross validation. Thus, the accuracies of the predictions for each VOC were taken for the 4 possible permutations of training and validation sets, whereby 3 different batches were used to train and 1 batch to validate (Figure 9). Looking at the overall tendency, fish gelatin-based films provided more accurate predictions when compared to bovine gelatin ones. In particular, the frequency of correct predictions of hydrocarbons is dramatically larger when fish gelatin-based films are used for gas sensing (83.42% versus 60.92% obtained for bovine gelatin sensors). In turn, bovine gelatin-based films could accurately predict acetone and ethanol in a higher frequency than fish gelatin-based sensors. Even though firm conclusions cannot be taken because of some variability between batches and analysis methods, these variations might be related to the structural differences between bovine and fish gelatin. The larger content of proline and hydroxyproline in bovine gelatin could eventually increase its affinity to polar VOCs as ethanol.

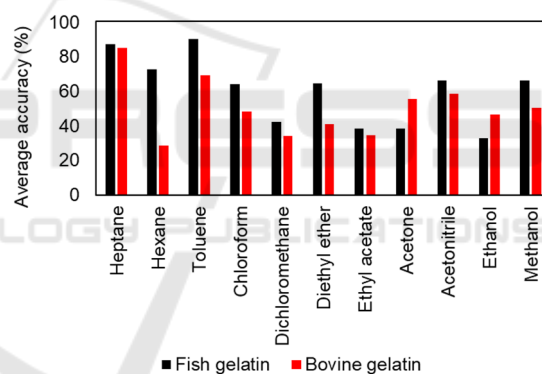


Figure 9: Comparison of average accuracies, for each VOC, when using fish gelatin and bovine gelatin-based sensors. The correct predictions of 4 different analyses were averaged. In average, the accuracy of fish gelatin sensors was 60.36% while the one of bovine gelatin sensors was 50.23%.

4 CONCLUSIONS

In summary, we present a new class of gas-sensing films based on self-assembled liquid crystal/ionic liquid droplets within a fish gelatin matrix. The produced homogeneous films have shown to be stable throughout 1 month, despite some droplet slight changes in the first week due to relative humidity fluctuations. We here show that, when using these gas-sensing films, some volatile organic compounds have characteristic optical signals, leading to good

accuracies upon prediction of the sensed volatile, especially for the discrimination of hydrocarbons or for the distinction of the alcohols chemical class.

The gel production and sensing experiment was reproducible, even though it was showed that the films cannot be reused. Since the main morphological changes happened after the first exposure to the set of 11 VOCs, the prediction accuracy increased for some VOCs in the third exposure, e.g. chloroform.

The lack of birefringence and optical response when using the controls without LC as sensor was expected and reassures the key role of LC as the optical probe. In turn, the importance of ionic liquids with surfactant-like properties is also proved by the control without IL, which detects VOCs but not in a very consistent way due to the absence of droplets' radial configuration.

Fish gelatin appeared as an alternative to bovine gelatin to encapsulate LC/IL droplets and form stimuli-responsive biosensors. Fish gelatin-based films showed slightly higher capability to correctly predict VOCs. Other biopolymeric matrices are being investigated to create an array of sensors that enhances selectivity for optoelectronic devices.

ACKNOWLEDGEMENTS

This project has received funding from the European Research Council (ERC) under the EU Horizon 2020 research and innovation programme (grant agreement No. SCENT-ERC-2014-STG-639123). This work was supported by the Applied Molecular Biosciences Unit – UCIBIO, which is financed by national funds from FCT/MCTES (UID/Multi/04378/2020).

REFERENCES

- Baldwin, E. A., Bai, J., Plotto, A., & Dea, S. (2011, May 2). Electronic noses and tongues: Applications for the food and pharmaceutical industries. *Sensors*, Vol. 11, pp. 4744–4766. <https://doi.org/10.3390/s110504744>
- Barbosa, A. J. M., Oliveira, A. R., & Roque, A. C. A. (2018, December 1). Protein- and Peptide-Based Biosensors in Artificial Olfaction. *Trends in Biotechnology*, Vol. 36, pp. 1244–1258. <https://doi.org/10.1016/j.tibtech.2018.07.004>
- Carlton, R. J., Hunter, J. T., Miller, D. S., Abbasi, R., Mushenheim, P. C., Tan, L. N., & Abbott, N. L. (2013). Chemical and biological sensing using liquid crystals. *Liquid Crystals Reviews*, 1(1), 29–51. <https://doi.org/10.1080/21680396.2013.769310>
- Carvalho, T., Vidinha, P., Vieira, B. R., Li, R. W. C., & Gruber, J. (2014). Ion Jelly: A novel sensing material for gas sensors and electronic noses. *Journal of Materials Chemistry C*, 2(4), 696–700. <https://doi.org/10.1039/c3tc31496k>
- Esteves, C., Santos, G. M. C., Alves, C., Palma, S. I. C. J., Porteira, A. R., Filho, J., ... Roque, A. C. A. (2019). Effect of film thickness in gelatin hybrid gels for artificial olfaction. *Materials Today Bio*, 1, 100002. <https://doi.org/10.1016/j.mtbio.2019.100002>
- Gutiérrez, J., & Horrillo, M. C. (2014, June 15). Advances in artificial olfaction: Sensors and applications. *Talanta*, Vol. 124, pp. 95–105. <https://doi.org/10.1016/j.talanta.2014.02.016>
- Hussain, A., Semeano, A. T. S., Palma, S. I. C. J., Pina, A. S., Almeida, J., Medrado, B. F., ... Roque, A. C. A. (2017). Tunable Gas Sensing Gels by Cooperative Assembly. *Advanced Functional Materials*, 27(27), 1700803. <https://doi.org/10.1002/adfm.201700803>
- Joly-Duhamel, C., Hellio, D., & Djabourov, M. (2002). All gelatin networks: 1. Biodiversity and physical chemistry. *Langmuir*, 18(19), 7208–7217. <https://doi.org/10.1021/la020189n>
- Karim, A. A., & Bhat, R. (2009, May 1). Fish gelatin: properties, challenges, and prospects as an alternative to mammalian gelatins. *Food Hydrocolloids*, Vol. 23, pp. 563–576. <https://doi.org/10.1016/j.foodhyd.2008.07.002>
- Meng, Z., Zheng, X., Tang, K., Liu, J., & Qin, S. (2012). Dissolution of natural polymers in ionic liquids: A review. (028), 1–29.
- Mhd Sarbon, N., Badii, F., & Howell, N. K. (2013). Preparation and characterisation of chicken skin gelatin as an alternative to mammalian gelatin. *Food Hydrocolloids*, 30(1), 143–151. <https://doi.org/10.1016/j.foodhyd.2012.05.009>
- Rehman, A., & Zeng, X. (2015, July 3). Methods and approaches of utilizing ionic liquids as gas sensing materials. *RSC Advances*, Vol. 5, pp. 58371–58392. <https://doi.org/10.1039/c5ra06754e>
- Rueden, C. T., Schindelin, J., Hiner, M. C., DeZonia, B. E., Walter, A. E., Arena, E. T., & Eliceiri, K. W. (2017). ImageJ2: ImageJ for the next generation of scientific image data. *BMC Bioinformatics*, 18(1), 529. <https://doi.org/10.1186/s12859-017-1934-z>
- Santos, G., Alves, C., Pádua, A. C., Palma, S., Gamboa, H., & Roque, A. C. (2019). An optimized e-nose for efficient volatile sensing and discrimination. *BIODEVICES 2019 - 12th International Conference on Biomedical Electronics and Devices, Proceedings; Part of 12th International Joint Conference on Biomedical Engineering Systems and Technologies, BIOSTEC 2019*, 36–46. <https://doi.org/10.5220/0007390700360046>
- Schindelin, J., Arganda-Carreras, I., Frise, E., Kaynig, V., Longair, M., Pietzsch, T., ... Cardona, A. (2012, July 28). Fiji: An open-source platform for biological-image analysis. *Nature Methods*, Vol. 9, pp. 676–682. <https://doi.org/10.1038/nmeth.2019>
- Shibaev, P. V., Wenzlick, M., Murray, J., Tantillo, A., & Howard-Jennings, J. (2015). Rebirth of liquid crystals for sensoric applications: Environmental and gas sensors. *Advances in Condensed Matter Physics, 2015*. <https://doi.org/10.1155/2015/729186>